Novel conductive nanocomposites from perfluoropolyether waterborne polyurethanes and carbon nanotubes

Diego Molina, Gianmarco Griffini*, Marinella Levi and Stefano Turri

Received: 13 January 2014,
Revised: 21 May 2014,
Accepted: 22 May 2014,
Published online: 17 June 2014

INTRODUCTION

Since their discovery in 1991,[1] carbon nanotubes (CNTs) have attracted a great deal of scientific and industrial attention due to their outstanding mechanical properties, thermal stability, thermal and electrical conductivity. Their use as fillers in polymer-based nanocomposites has significantly increased the field of technological applications in which polymeric materials may be employed. In fact, even small concentrations of CNTs (in the order of few percents or even less) have been shown to have a significant impact on the modification of the properties of polymeric materials thanks to the large and tunable aspect ratio of CNTs that make them very effective compared with traditional carbon black micro or nanoparticles.[2–5] The excellent electrical conductivity of CNTs has been exploited for the preparation of conductive nanocomposites based on different classes of insulating polymers *via* the formation of a continuous network of conductive CNTs in the polymer matrix.[6–15] Progresses in the control of such network have led to significant improvements in the electrical conductivity of CNT/polymer nanocomposites. Accordingly, such systems have found applications in many advanced technological fields such as pressure, temperature and liquid/gas sensors, electrostatic dissipation and electromagnetic shielding materials, and electric heating systems.[16–22]

Fluorinated polymers are a class of highly performing materials that exploit the superior strength of the carbon-fluorine bond to achieve very peculiar properties such as high thermal stability, excellent chemical resistance, and outstanding weatherability. Among them, perfluoropolyether (PFPE) functional oligomers have been used as building blocks for the realization of high performance copolymers, mainly based on the polyurethane chemistry.[23–26] Thanks to these characteristics, these systems have been exploited in a variety of scientific and technological fields that include original equipment manufacturing coatings,[27,28] plastic coatings,[29] rubber seals,[30] and water/oil repellent finishings.[31,32] PFPE-based polyurethanes (PFPE-PUs) are normally employed as highly insulating materials. However, the addition of highly conductive fillers into such non-conductive polymeric systems may provide access to new technological and industrial fields where the unique water/oil repellency, low T_g, chemical resistance, and excellent substrate adhesion characteristics of PFPE-PUs need to be combined with the electrical conductivity or the electrostatic dissipation properties of CNTs. In particular, CNT/PFPE-PU nanocomposites may find potential applications in the printing industry as coatings

* *Correspondence to: Gianmarco Griffini, Department of Chemistry, Materials and Chemical Engineering "Giulio Natta", Politecnico di Milano, Piazza Leonardo da Vinci 32, 20133 Milano, Italy.*
E-mail: gianmarco.griffini@polimi.it

D. Molina, G. Griffini, M. Levi, S. Turri
Department of Chemistry, Materials and Chemical Engineering "Giulio Natta", Politecnico di Milano, Piazza Leonardo da Vinci 32, 20133 Milano, Italy

for printing rollers with improved and durable toner adhesion/transfer/release properties,[33–35] as well as in the field of energy storage and conversion as hydrophobic coatings for the gas diffusion layer in polymer electrolyte membrane fuel cells.[36] Despite the large number of publications investigating the mechanical and electrical properties of CNT/polymer nanocomposites, very few works are present in the literature concerning CNT-nanocomposites based on fluorinated polymers.[37,38] In addition, to the best of our knowledge, no specific studies on the investigation of CNT/PFPE-PU systems have been reported to date. However, a deeper understanding of the mechanical and electrical properties of CNT/PFPE-PU nanocomposite materials is needed in order to be fully exploited.

In this work, new nanocomposites based on waterborne PFPE-PU and increasing amounts of multi-walled (MW) CNTs bearing carboxylated functional groups (COOH-CNTs) were prepared and characterized for the first time. A methodology for the preparation of the nanocomposites was developed allowing to obtain excellent reproducibility at all COOH-CNT concentrations investigated. The effect of increasing concentration of COOH-CNTs on the physical and mechanical properties of the nanocomposites was investigated by means of rheological measurements, dynamic mechanical analysis and thermal characterization. Optical contact angle (OCA) measurements were used to examine the wettability behavior of the COOH-CNT/PFPE-PU systems and were correlated with scanning electron microscopy analysis of the surface of the nanocomposites. The electrical insulating behavior of the pristine PFPE-PU system was shown to undergo substantial modifications upon addition of COOH-CNTs, leading to the formation of conductive systems with electrical conductivities as high as 1 S/cm for high COOH-CNT loading and a percolation threshold concentration of 0.98 wt%.

The ultimate aim of this study is to demonstrate that the addition of CNTs to insulating PFPE-PU matrices allows to prepare conducting nanocomposite materials with very peculiar properties that may find application in specialized technological fields where excellent chemical stability, hydrophobic/oleophobic character, better mechanical properties, and electrical conductivity are simultaneously required.

EXPERIMENTAL

Materials

The preparation of the waterborne PFPE-PUs used in this study is based on a process described elsewhere (see Figure S1 in the Supporting Information for the molecular structure).[31] Such system is an aqueous dispersion of an anionic segmented PU containing PFPE blocks and carboxylate functional side groups with a solid content of 26% w/w and a molecular weight of about 20,000 g/mol. Carboxylated MWCNTs (Nanocyl NC 3101, Nanocyl) having average diameter of 9.5 nm and average length of 1.5 μm were employed for the preparation of fluorinated nanocomposites because of their better compatibility with aqueous media compared with non-functionalized MWCNTs. All other chemicals were provided by Sigma Aldrich, unless otherwise stated.

Preparation of nanocomposite dispersion

Each PFPE-PU dispersion was diluted with deionized water to reach a final solid content of 10% w/w and magnetically stirred at 600 rpm for 30 min prior to further processing to create a homogenous and stable diluted aqueous dispersion. The desired amount of COOH-CNTs (1–10 wt%) was added to 100 ml of such diluted PFPE-PU aqueous dispersion, followed by mixing under magnetic stirring at 950 rpm for 30 min. The so-obtained COOH-CNT/PFPE-PU dispersion was then placed in an ultrasonic bath (Starsonic 90) at room temperature for 1 hr. Finally, the COOH-CNT/PFPE-PU dispersion was ultrasonicated by means of a Sonic & Materials VCX130 sonicator tip for 30 min. This last step was carried out in an ice bath in order to compensate for the exothermicity arising from the ultrasonication process and to prevent water evaporation from the dispersion. This procedure allowed to reproducibly obtain stable COOH-CNT/PFPE-PU aqueous dispersions (in the text referred to as P-CNT-X, where X denotes the wt% of COOH-CNT present in the nanocomposite) that retain their stability for more than a year after the first preparation.

Characterization

Rheological measurements were performed using a Rheometrics DSR200 rheometer with a 25 mm plate-cone configuration at 25°C. Steady shear tests on COOH-CNT/PFPE-PU dispersions were performed for 3 min in the 0–120 Pa range. Differential scanning calorimetry (DSC) measurements were performed by means of a Mettler-Toledo DSC/823e (10-30 K/min scan rate, −140–200°C temperature range, N_2 environment) on 0.1 mm thick solid state samples obtained by drop casting the COOH-CNT/PFPE-PU aqueous dispersions on poly(tetrafluoroethylene) plates followed by drying in air for 48 hr at 40°C and subsequent heating in an air-forced oven at 100°C for 24 hr (until constant weight was achieved). Values reported were obtained from the second run. Dynamic mechanical analysis (DMA) was performed on 0.1 mm thick circular samples with a diameter of 0.5 cm using a Mettler DMA/SDTA861e dynamic mechanical analyzer in shear-sandwich mode. Dynamic scans were conducted from −30°C to 180°C at increasing oscillatory frequencies (0.5, 1, 5, and 10 Hz), maintaining a specimen deformation lower than 0.5%. All samples were re-clamped before starting the scan at −30°C to counteract the thermal shrinkage. OCA measurements on the COOH-CNT/PFPE-PU nanocomposites were performed by means of an OCA 20 (DataPhysics) equipped with a CCD photo-camera and with a 500 μl Hamilton syringe to dispense liquid droplets. Water and diiodomethane were used as probe liquids in static measurements that were taken at room temperature via the sessile drop technique. At least 30 measurements were performed in different regions on the surface of each sample and the results were averaged. Dynamic (advancing and receding contact angle) measurements were also performed on COOH-CNT/PFPE-PU nanocomposites using water as probe liquid (three advancing-receding cycles with a delivered volume of 1 μl), and the results were averaged out of at least 15 measurements. The surface roughness of COOH-CNT/PFPE-PU nanocomposites was measured by optical profilometry (Microfocus, UBM) and expressed as root mean square surface roughness (R_{RMS}). Scanning electron microscopy (SEM) was performed using a Cambridge Stereoscan 360 scanning electron microscope (acceleration voltage of 0.2–40 kV) on 0.1 mm thick nanocomposite films to evaluate their surface morphology and the surface distribution of COOH-CNTs. Electrical measurements were performed on 25 mm (length) × 10 mm (width)× 0.1 mm (thickness) samples using a Keithley 2612 digital source-measure unit. To achieve a uniform electric field within the samples, spring-

loaded needle point probes (SPP4 S/F, Multi Contact) were put into contact with each $10 \times 0.1\,mm^2$ sample edge previously painted with silver-based conductive paint to improve the electrical contact. A voltage scan between 0.1 and 200 V was applied on each sample with 4 V steps and a measuring time of 20 sec for each step. This testing procedure was chosen to reduce the R–C circuit behavior observed in most of the samples when a fast voltage change was applied. Conductivity of the nanocomposites was then calculated from resistance measurements.

RESULTS AND DISCUSSION

Rheological measurements

Obtaining a uniform homogeneous dispersion of MWCNTs within a polymeric matrix is a challenge, because of the high tendency of MWCNTs to form bundles and aggregates.[39,40] For this reason, the evaluation of the quality of the dispersion represents a key factor for the development of high performing MWCNT-based polymer nanocomposites. In this context, rheology represents a powerful tool to assess the quality of the dispersion process and to characterize the distribution of MWCNTs and their interactions with the polymeric matrix.[41–43] In this work, steady shear rheological measurements were employed to evaluate the quality of the dispersion process. Accordingly, the experimental method used in this work for the preparation of the nanocomposite dispersions was found to give excellent reproducibility of the dispersion, as shown by rheological tests carried out on samples obtained from different batches by using the same procedure (Figure S2 in the Supporting Information). In order to monitor the effects of the addition of COOH-CNTs to the fluorinated polymer matrix, the rheological behavior of COOH-CNT/PFPE-PU nanocomposites was investigated at increasing COOH-CNT content, and the results are presented in Fig. 1.

As shown in the plot, the undoped PFPE dispersion (P-CNT-0) shows a Newtonian behavior, as a consequence of the large amount of water present (90 wt%). On the other hand, the viscosity of the COOH-CNT/PFPE-PU dispersions increases at increasing COOH-CNT concentration and results in a shear thinning behavior, more visible at low shear rate values, even for very low COOH-CNT concentrations. In addition, a sharp increase in viscosity compared with the neat PFPE-PU matrix is already observed for a COOH-CNT concentration of 1 wt% (P-CNT-1). This modification of the rheological behavior upon addition of COOH-CNTs is well documented in the literature for nanocomposites based on different polymer matrices[8,41,43] and is often ascribed to the formation of an interconnected network of CNTs in the nanocomposite above a CNT threshold concentration (in this case, around 1 wt%). Such network partially prevents the polymer matrix from flowing and leads to a characteristic gel-like behavior.

Rheological measurements were also carried out on P-CNT-10, but they gave poor reproducibility, likely due to the high viscosities of this highly loaded nanocomposite which tend to entrap air bubbles during processing

Table 1. Glass transition temperatures of the nanocomposites at increasing COOH-CNT concentration

	COOH-CNT concentration [% wt.]	T_g^F [°C]	T_g^H [°C]
P-CNT-0	0	−81	51
P-CNT-1	1	−73	61
P-CNT-3	3	−74	63
P-CNT-5	5	−77	66
P-CNT-10	10	−77	70

T_g^F is the glass transition temperature of the fluorinated phase. T_g^H is the glass transition temperature of the hard urethane phase.

Differential scanning calorimetry

Differential scanning calorimetry analysis was used to evaluate the thermal transitions in the COOH-CNT/PFPE-PU nanocomposites. Table 1 presents the values of glass transition (T_g) temperature at increasing COOH-CNT concentration. Because of the presence of urethane moieties, the corresponding nanocomposites showed two distinct glass transitions that can be ascribed to the nanoscale segregation of the PFPE phase and the urethane phase resulting from their different solubility parameters.[25,31] In particular, the lower T_g value is related to the soft fluorinated phase (T_g^F), while the higher T_g value is associated to the hydrogenated urethane phase (T_g^H).

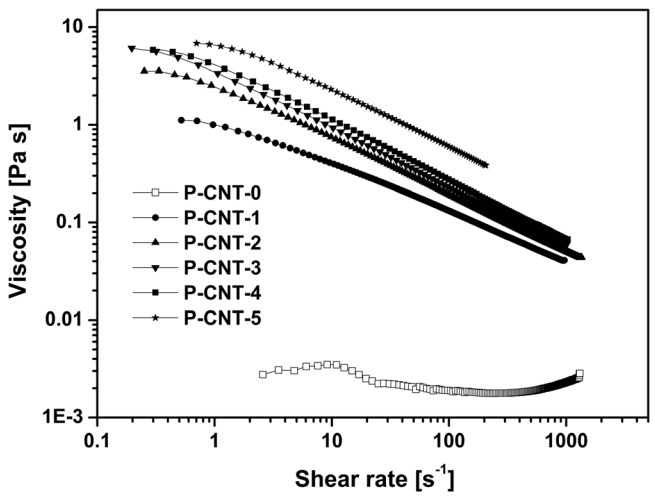

Figure 1. Steady shear rate curves at 25°C of P-CNT dispersions at increasing COOH-CNT concentrations.

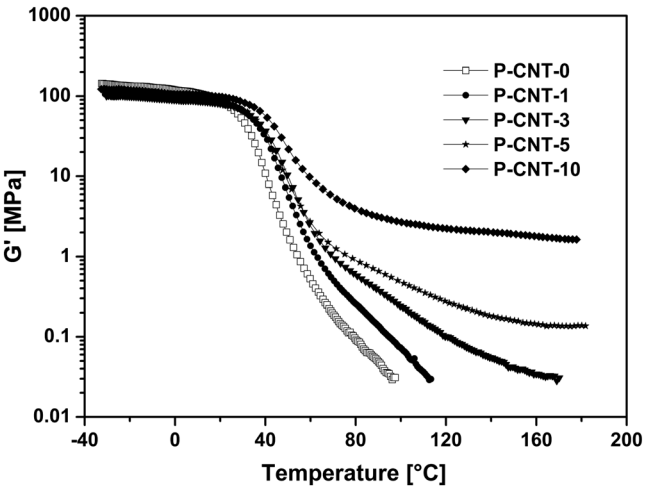

Figure 2. Storage modulus G′ as a function of temperature at 0.5 Hz for the nanocomposites at increasing COOH-CNT concentration.

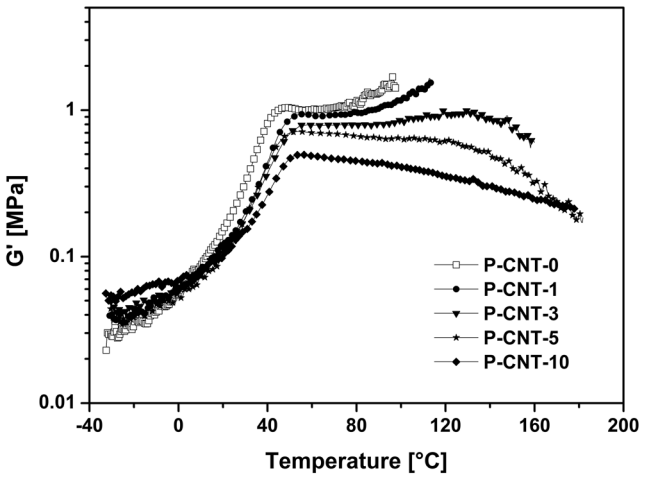

Figure 3. Loss factor tanδ (=G″/G′) as a function of temperature at 0.5 Hz for the nanocomposites at increasing COOH-CNT concentration.

Accordingly, the neat PFPE-PU polymer (P-CNT-0) shows a T_g^F value of −81°C and a T_g^H of 51°C. Upon addition of COOH-CNTs to the PFPE-PU, no obvious trends are observed on T_g^F that only undergoes a slight increase. As opposed to this, a much sharper increase is observed in T_g^H with COOH-CNTs concentration. In particular, T_g^H rises by about 20°C when 10 wt% COOH-CNTs are added (P-CNT-10). The different behavior observed on T_g^F and T_g^H upon COOH-CNT addition suggests that COOH-CNTs manifest a better affinity with the hydrogenated urethane chains compared with the fluorinated chains, likely because of the presence of carboxylic groups on the CNT external walls. This stronger interaction with the hard urethane phase may be responsible for the sharp increase in T_g^H.

Dynamic mechanical analysis

In order to assess the effect of the addition of COOH-CNTs on the mechanical properties of the PFPE-PU polymeric matrix, DMA was performed. Figure 2 shows the temperature dependence of the storage modulus (G′) at 0.5 Hz for the nanocomposites at increasing COOH-CNT content. A plateau value for G′ of about 100 MPa is observed in the 0–30°C temperature range that does not appear to be affected by the addition of COOH-CNTs. A similar behavior is found at different scanning frequencies (Figure S3 in the Supporting Information). As the concentration of COOH-CNTs is increased, a rubbery plateau is also observed above the relaxation temperature (T > 70°C), more evident for highly doped nanocomposites (P-CNT-10). G′ values on this rubbery plateau are found to increase as the COOH-CNT concentration is increased, with values as high as 3 MPa for P-CNT-10. In particular, the presence of COOH-CNTs in highly doped nanocomposites allows to extend the rubbery plateau to a significantly higher temperature range compared to the pristine PFPE-PU system (P-CNT-0). This behavior may allow to exploit the peculiar mechanical properties of PFPE-PU systems also in high temperature applications. The addition of COOH-CNTs also causes a broadening of the glass-to-rubber relaxation that is found to extend for about 30°C in highly doped systems. Such broadening at increasing COOH-CNT content can be related to the distribution of relaxation times in the PFPE-PU nanocomposites.

In order to further investigate this effect, the loss factor tanδ (=G″/G′) dependence on temperature was monitored at increasing COOH-CNT content, and the results are presented in Fig. 3. Clearly, as the concentration of COOH-CNTs is increased, the tanδ peak broadens significantly toward higher temperatures, this effect being more evident for highly doped nanocomposites.

This behavior may indicate that at higher COOH-CNT loading, a more efficient interaction between COOH-CNTs and polymer chains is occurring. This stronger interaction may significantly change the relaxation times distribution.

In addition to an increase in the tanδ peak width, a reduction of tanδ peak intensity is also found, as reported in Table 2, where results obtained from different scan frequencies are reported. Such a decrease in tanδ peak intensity with increasing COOH-CNT concentration may be explained by considering the COOH-CNT/PFPE-PU and COOH-CNT/COOH-CNT interactions within the nanocomposite.[44–46] By increasing the COOH-CNT concentration in the PFPE-PU polymer matrix, the distance between COOH-CNTs decreases and a three-dimensional network of COOH-CNT aggregates is formed. Part of the polymer matrix may get trapped in such aggregates, thus resulting in the presence of low-mobility polymer chains within the COOH-CNT network. This three-dimensional network leads to a substantial increase in the effective volume fraction of filler, as both COOH-CNTs and polymer matrix trapped in the COOH-CNT agglomerates need to be taken into account. As a result, the elastic modulus increases while the hysteresis (tanδ peak intensity) decreases. As shown in Table 2, this effect does not appear to be affected by the scan frequency, suggesting that the specific interactions between filler and polymer matrix do not change by increasing the stress state.

Optical contact angle

The surface properties of the COOH-CNT/PFPE-PU nanocomposites were investigated by means of static contact angle measurements with water and diiodomethane, and the surface tension γ of each sample, together with its dispersive γ^d and polar γ^p components, was calculated using the Wu harmonic mean approximation.[47]

Table 2. Values of tanδ peak intensity obtained from dynamic mechanical analysis measurements at different scanning frequencies (0.5–10 Hz) for the nanocomposites with increasing amount of COOH-CNTs

	COOH-CNT concentration [wt%]	tanδ peak value at 0.5 Hz [-]	tanδ peak value at 1 Hz [-]	tanδ peak value at 5 Hz [-]	tanδ peak value at 10 Hz [-]
P-CNT-0	0	1.04	1.02	0.96	0.95
P-CNT-1	1	0.94	0.93	0.88	0.86
P-CNT-3	3	0.79	0.79	0.75	0.75
P-CNT-5	5	0.72	0.71	0.68	0.66
P-CNT-10	10	0.50	0.50	0.47	0.46

Table 3. Static contact angles (θ_{H2O}, θ_{CH2I2}), total surface tension (γ) with its dispersive (γ^d) and polar (γ^p) components, and difference between advancing and receding dynamic contact angles ($\Delta\theta_{H2O}$) for the nanocomposites at increasing COOH-CNT concentration

	θ_{H2O} [°]	θ_{CH2I2} [°]	γ [mN/m]	γ^d [mN/m]	γ^p [mN/m]	$\Delta\theta_{H2O}$ [°]
P-CNT-0	111.9 ± 0.9	95.2 ± 1.6	16.7 ± 0.5	13.1 ± 0.7	3.6 ± 0.3	51.4 ± 1.9
P-CNT-1	111.7 ± 0.6	94.3 ± 1.0	16.7 ± 0.4	13.5 ± 0.3	3.2 ± 0.5	51.0 ± 2.5
P-CNT-3	111.6 ± 0.7	94.4 ± 0.8	16.7 ± 0.5	13.5 ± 0.4	3.3 ± 0.4	51.0 ± 3.2
P-CNT-5	112.7 ± 0.9	96.5 ± 1.1	16.0 ± 0.3	12.7 ± 0.2	3.2 ± 0.3	55.3 ± 3.0
P-CNT-10	118.6 ± 1.2	100.2 ± 1.6	13.6 ± 0.9	11.9 ± 0.8	1.8 ± 0.9	62.0 ± 3.0

As presented in Table 3, all nanocomposites show high values of static contact angles against water (θ_{H2O}) and diodomethane (θ_{CH2I2}), confirming the highly hydrophobic/oleophobic nature of these systems. In addition, a slight increase in θ_{H2O} and θ_{CH2I2} is observed with COOH-CNT concentration, leading to a corresponding decrease in surface energy γ from 17 mN/m for P-CNT-0 to 14 mN/m for P-CNT-10. This behavior may be explained in terms of the Wenzel model for hydrophobicity[48] by taking into account the increased root mean square surface roughness R_{RMS} of these systems at high COOH-CNT concentration. In particular, an R_{RMS} value of 50 nm is found in pristine coatings (P-CNT-0), as opposed to the significantly higher R_{RMS} reported on P-CNT-5 systems (228 nm). These observations are further supported by dynamic contact angle measurements on the same systems by evaluating the difference between advancing and receding contact angles using water as probe liquid ($\Delta\theta_{H2O}$). As observed in Table 3, an increase of $\Delta\theta_{H2O}$ of about 10° is observed with increasing COOH-CNT concentration, which can be related to the rougher surface morphology found in highly doped nanocomposites.

Scanning electron microscopy

Undoped PFPE-PU polymer and COOH-CNT/PFPE-PU nanocomposites were also investigated by SEM. As shown in Fig. 4a, pristine P-CNT-0 system shows a very plain and smooth surface morphology. With the addition of COOH-CNTs, an increase in surface roughness is clearly observed (Fig. 4b). In addition, by examination of the fracture surface of cryo-fractured COOH-CNT/PFPE-PU samples (Fig. 4c and d), it appears that a good level of dispersion and distribution of COOH-CNTs into the PFPE-PU polymer matrix is obtained, even at high COOH-CNT content.

Electrical conductivity

The volume electrical conductivity σ of COOH-CNT/PFPE-PU nanocomposites was measured at increasing COOH-CNT concentration, and the results are presented in Fig. 5. As expected, the highly insulating character of the polymer matrix can be modified with the introduction of COOH-CNTs. In particular, conductivity σ is found to progressively increase with COOH-CNT concentration until values in the order of 1 S/cm are reached for highly doped (10 wt%) nanocomposites, following a typical percolation behavior. Results on non-fluorinated waterborne PU systems containing MWCNTs showed maximum electrical conductivities in the order of 10^{-3}–10^{-4} S/cm.[13,22,49] More recently, higher values of electrical conductivities in the 1–4 S/cm range were obtained in composites based on aramids,[19] polyaniline[50] or thiophene derivatives,[51] and MWCNTs. On the basis of these considerations and on the electrical conductivities obtained in the present study, the

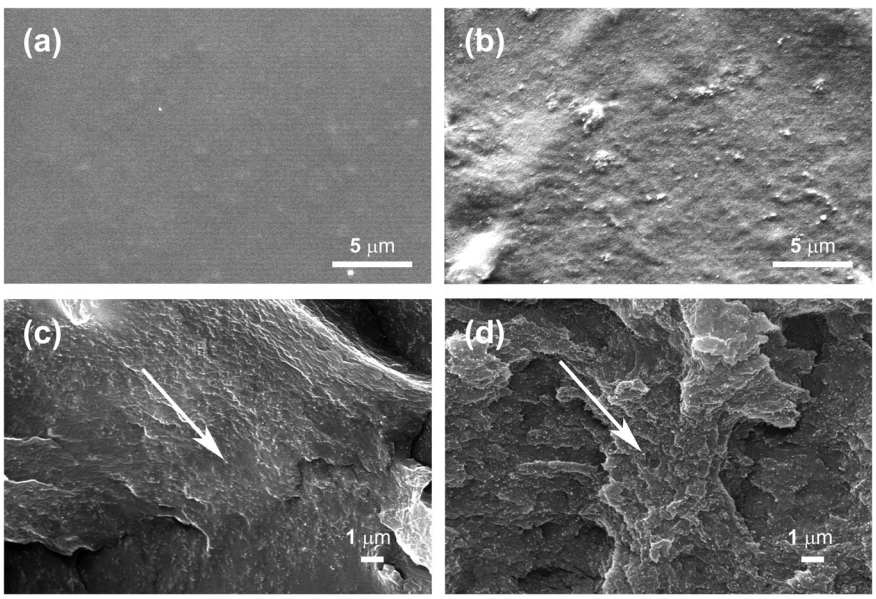

Figure 4. Surface morphology of (a) P-CNT-0 and (b) P-CNT-5 nanocomposites, and fracture morphology of (c) P-CNT-1 and (d) P-CNT-5 nanocomposites, as shown by scanning electron microscopy analysis. The arrows indicate the white dots that can be associated with the presence of COOH-CNTs.

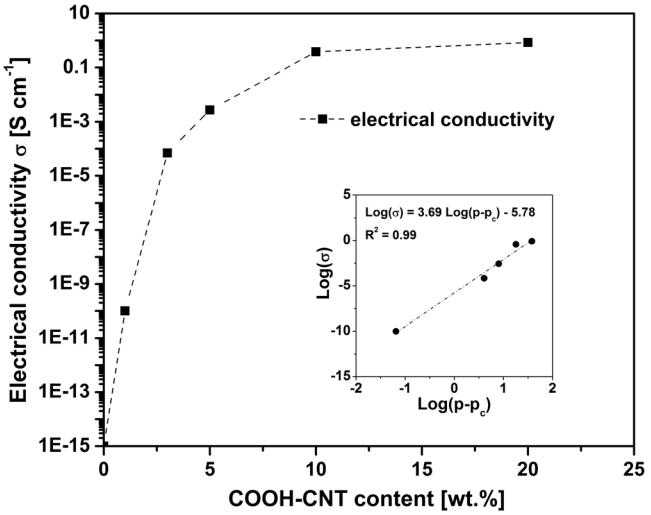

Figure 5. Volume electrical conductivity as a function of COOH-CNT concentration for the systems investigated in this work. The inset shows the log-log plot of the electrical conductivity versus the volume fraction of COOH-CNTs.

fluoropolymer-based systems developed in this work represent a very promising platform to achieve conductive nanocomposites.

To determine the electrical percolation threshold, the following power law was used:[52]

$$\sigma \propto (p - p_C)^{\alpha} \quad (1)$$

where σ is the electrical conductivity, p is the COOH-CNT volume concentration and p_c is the critical COOH-CNT volume concentration at electrical percolation and α is a critical exponent. As shown in the inset to Fig. 5, a good fit to the experimental values of log(σ) versus log($p - p_c$) was given by a percolation threshold concentration of 0.98 wt% and $\alpha = 3.69$. These values are in line with reports recently presented on different systems, where it was found that α values as high as 4 can be obtained in MWCNT-polymer nanocomposites and that both p_c and α are highly dependent on the morphology and aspect ratio of the filler.[53]

CONCLUSIONS

In this work, new PFPE-PU based nanocomposites containing increasing amount of carboxylated (COOH-) CNTs were prepared and characterized. Rheological characterization of the nanocomposite dispersions evidenced a clear shear thinning behavior for all systems containing COOH-CNTs, as opposed to the undoped PFPE-PU matrices that showed a Newtonian behavior. Thermal characterization of the COOH-CNT/PFPE-PU nanocomposites indicated that the addition of COOH-CNTs does not significantly affect the glass transition temperatures of the pristine PFPE-PU matrices, allowing to preserve the peculiar thermal properties of these materials. Dynamic mechanical analysis on fluorinated polyurethane nanocomposites showed that G' values exceeding 3 MPa could be obtained in highly doped nanocomposites (10 wt % COOH-CNT). This behavior may allow to exploit the peculiar mechanical properties of PFPE-PU systems also in high temperature applications not accessible to undoped systems. In addition, the surface properties of the COOH-CNT/PFPE-PU nanocomposites were found to well correlate with their surface morphology, as evidenced by static and dynamic contact angle measurements and SEM analysis. The addition of COOH-CNTs was shown to modify the highly insulating character of the pristine PFPE-PU system, leading to the formation of conductive nanocomposites with σ values as high as 1 S/cm for high COOH-CNT loading and a percolation threshold concentration of 0.98 wt%.

The results of this study demonstrate for the first time that the addition of COOH-CNTs to PFPE-PU systems represents a promising strategy to expand their possible use to technological applications where chemical stability, water/oil repellence and electrical conductivity are simultaneously required.

REFERENCES

[1] S. Iijima, *Nature* **1991**, *354*, 56–58.
[2] J. N. Coleman, U. Khan, Y. K. Gun'ko, *Adv. Mater.* **2006**, *18*, 689–706.
[3] J. N. Coleman, U. Khan, W. J. Blau, Y. K. Gun'ko, *Carbon* **2006**, *44*, 1624–1652.
[4] M. M. J. Treacy, T. W. Ebbesen, J. M. Gibson, *Nature* **1996**, *381*, 678–680.
[5] D. F. Wu, L. Wu, W. D. Zhou, Y. R. Sun, M. Zhang, *J. Polym. Sci. Polym. Phys.* **2010**, *48*, 479–489.
[6] F. M. Du, R. C. Scogna, W. Zhou, S. Brand, J. E. Fischer, K. I. Winey, *Macromolecules* **2004**, *37*, 9048–9055.
[7] K. I. Winey, T. Kashiwagi, M. F. Mu, *MRS Bull.* **2007**, *32*, 348–353.
[8] M. Abdalla, D. Dean, P. Robinson, E. Nyairo, *Polym.* **2008**, *49*, 3310–3317.
[9] M. J. Kayatin, V. A. Davis, *Macromolecules* **2009**, *42*, 6624–6632.
[10] S. Isaji, Y. Z. Bin, M. Matsuo, *Polym.* **2009**, *50*, 1046–1053.
[11] S. Kara, E. Arda, F. Dolastir, O. Pekcan, *J. Colloid Interface Sci.* **2010**, *344*, 395–401.
[12] G. D. Seidel, A. S. Puydupin-Jamin, *Mech. Mater.* **2011**, *43*, 755–774.
[13] J. Y. Kwon, H. D. Kim, *J. Appl. Polym. Sci.* **2005**, *96*, 595–604.
[14] S. H. Choi, D. H. Kim, A. V. Raghu, K. R. Reddy, H.-I. Lee, K. S. Yoon, H. M. Jeong, B. K. Kim, *J. Macromol. Sci. Phys.* **2012**, *51*, 197–207.
[15] D. A. Nguyen, A. V. Raghu, J. T. Choi, H. M. Jeong, *Polym. Polym. Compos.* **2010**, *18*, 351–358.
[16] J. M. Thomassin, X. Lou, C. Pagnoulle, A. Saib, L. Bednarz, I. Huynen, R. Jerome, C. Detrembleur, *J. Phys. Chem. C* **2007**, *111*, 11186–11192.
[17] J. I. Lee, S. B. Yang, H. T. Jung, *Macromolecules* **2009**, *42*, 8328–8334.
[18] M. H. Al Saleh, U. Sundararaj, *Carbon* **2009**, *47*, 1738–1746.
[19] H. C. Neitzert, L. Vertuccio, A. Sorrentino, *IEEE T. Nanotech.* **2011**, *10*, 688–693.
[20] S. M. Shang, W. Zeng, X. M. Tao, *Sens. Actuators B* **2012**, 166, 330–337.
[21] Y. G. Jeong, G. W. Jeon, *ACS Appl. Mater. Interfaces* **2013**, *5*, 6527–6534.
[22] H. He, X. B. Xu, D. F. Zhang, *Sens. Actuators B* **2013**, *176*, 940–944.
[23] S. Turri, S. Radice, R. Canteri, G. Speranza, M. Anderle, *Surf. Interface Anal.* **2000**, *29*, 873–886.
[24] S. Turri, M. Levi, M. Cristini, A. Sanguineti, *Polym. Int.* **2005**, *54*, 698–704.
[25] S. Turri, R. Valsecchi, M. Levi, M. Cristini, A. Sanguineti, *Eur. Polym. J.* **2008**, *44*, 2951–2961.
[26] M. Licchelli, S. J. Marzolla, A. Poggi, C. Zanchi, *J. Cult. Heritage* **2011**, *12*, 34–43.
[27] G. Simeone, S. Turri, M. Scicchitano, C. Tonelli, *Angew. Makromol. Chem.* **1996**, *236*, 111–127.
[28] S. Turri, M. Scicchitano, G. Simeone, C. Tonelli, *Prog. Org. Coat.* **1997**, *32*, 205–213.
[29] A. Di Gianni, R. Bongiovanni, A. Priola, S. Turri, *Int. J. Adhes. Adhes.* **2004**, *24*, 513–518.
[30] S. Turri, M. Levi, M. Cristini, A. Sanguineti, *J. Polym. Res.* **2007**, *14*, 141–145.
[31] T. Trombetta, P. Iengo, S. Turri, *J. Appl. Polym. Sci.* **2005**, *98*, 1364–1372.
[32] R. Canteri, G. Speranza, M. Anderle, S. Turri, S. Radice, *Surf. Interface Anal.* **2003**, *35*, 318–326.
[33] J. Lahti, A. Savolainen, J. P. Rasanen, T. Suominen, H. Huhtinen, *Polym. Eng. Sci.* **2004**, *44*, 2052–2060.
[34] D. S. Rimai, K. Brown, M. C. Zaretsky, K. Lofftus, M. Aslam, W. Y. Fowlkes, D. S. Weiss, *J. Adhes. Sci. Technol.* **2010**, *24*, 583–617.
[35] M. Satoh, S. Matsumoto, T. Higashiguchi, M. Matsuda, T. Muranoi, I. Kikuma, Y. Momose, M. Takeuchi, *Appl. Surf. Sci.* **1996**, *92*, 635–638.
[36] P. G. Stampino, D. Molina, L. Omati, S. Turri, M. Levi, C. Cristiani, G. Dotelli, *J. Power. Sources* **2011**, *196*, 7645–7648.
[37] T. T. Pham, V. Sridhar, J. K. Kim, *Polym. Compos.* **2009**, *30*, 121–130.

[38] X. Zhao, A. A. Koos, B. T. T. Chu, C. Johnston, N. Grobert, P. S. Grant, *Carbon* **2009**, *47*, 561–569.
[39] X. L. Xie, Y. W. Mai, X. P. Zhou, *Mater. Sci. Eng. R* **2005**, *49*, 89–112.
[40] Z. Spitalsky, D. Tasis, K. Papagelis, C. Galiotis, *Prog. Polym. Sci.* **2010**, *35*, 357–401.
[41] M. Chapartegui, N. Markaide, S. Florez, C. Elizetxea, M. Fernandez, A. Santamaria, *Compos. Sci. Technol.* **2010**, *70*, 879–884.
[42] I. Alig, T. Skipa, D. Lellinger, P. Potschke, *Polym.* **2008**, *49*, 3524–3532.
[43] Z. H. Fan, S. G. Advani, *J. Rheol.* **2007**, *51*, 585–604.
[44] J. Frohlich, W. Niedermeier, H. D. Luginsland, *Compos. Part A Appl. Sci.* **2005**, *36*, 449–460.
[45] J. L. Leblanc, *Prog. Polym. Sci.* **2002**, *27*, 627–687.
[46] G. Griffini, R. Suriano, S. Turri, *Polym. Eng. Sci.* **2012**, *52*, 2543–2551.
[47] S. Wu, *J. Colloid Interface Sci.* **1979**, *71*, 605–609.
[48] G. Whyman, E. Bormashenko, T. Stein, *Chem. Phys. Lett.* **2008**, *450*, 355–359.
[49] J. Y. Kwon, H. D. Kim, *J. Polym. Sci. Polym. Chem.* **2005**, *43*, 3973–3985.
[50] I. Brook, G. Mechrez, R. Y. Suckeveriene, R. Tchoudakov, M. Narkis, *Polym. Adv. Technol.* **2013**, *24*, 758–763.
[51] K. R. Reddy, H. M. Jeong, Y. Lee, A. V. Raghu, *J. Polym. Sci. Polym. Chem.* **2010**, *48*, 1477–1484.
[52] I. Balberg, *Carbon* **2002**, *40*, 139–143.
[53] W. Bauhofer, J. Z. Kovacs, *Compos. Sci. Technol.* **2009**, *69*, 1486–1498.

SUPPORTING INFORMATION

Additional supporting information may be found in the online version of this article at the publisher web-site